Absence of S6K1 protects against age- and diet-induced obesity while enhancing insulin sensitivity

Sung Hee Um[1], Francesca Frigerio[1], Mitsuhiro Watanabe[2], Frédéric Picard[2]*, Manel Joaquin[1], Melanie Sticker[1], Stefano Fumagalli[1], Peter R. Allegrini[3], Sara C. Kozma[1]*, Johan Auwerx[2] & George Thomas[1]

[1]*Friedrich Miescher Institute for Biomedical Research, Maulbeerstrasse 66, 4058 Basel, Switzerland*
[2]*Institut de Génétique et de Biologie Moléculaire et Cellulaire, CNRS/INSERM/ULP, and Institut Clinique de la Souris, Génopole Strasbourg, 67404 Illkirch, France*
[3]*Novartis Pharma AG, Klybeckstrasse 141, 4057 Basel, Switzerland*

* Present address: Laval Hospital Research Center, 2725 chemin Ste-Foy, Ste-Foy, Quebec G1V 4G5, Canada (F.P.); Genome Research Institute, University of Cincinnati, 2180 E. Galbraith Road, Cincinnati, Ohio 45237, USA (S.C.K.)

Elucidating the signalling mechanisms by which obesity leads to impaired insulin action is critical in the development of therapeutic strategies for the treatment of diabetes[1]. Recently, mice deficient for S6 Kinase 1 (S6K1), an effector of the mammalian target of rapamycin (mTOR) that acts to integrate nutrient and insulin signals[2], were shown to be hypoinsulinaemic, glucose intolerant and have reduced β-cell mass[3]. However, *S6K1*-deficient mice maintain normal glucose levels during fasting, suggesting hypersensitivity to insulin[3], raising the question of their metabolic fate as a function of age and diet. Here, we report that *S6K1*-deficient mice are protected against obesity owing to enhanced β-oxidation. However on a high fat diet, levels of glucose and free fatty acids still rise in *S6K1*-deficient mice, resulting in insulin receptor desensitization. Nevertheless, *S6K1*-deficient mice remain sensitive to insulin owing to the apparent loss of a negative feedback loop from S6K1 to insulin receptor substrate 1 (IRS1), which blunts S307 and S636/S639 phosphorylation; sites involved in insulin resistance[4,5]. Moreover, wild-type mice on a high fat diet as well as *K/K A^y* and *ob/ob* (also known as *Lep/Lep*) mice—two genetic models of obesity—have markedly elevated S6K1 activity and, unlike *S6K1*-deficient mice, increased phosphorylation of IRS1 S307 and S636/S639. Thus under conditions of nutrient satiation S6K1 negatively regulates insulin signalling.

As animals reach adulthood their growth rate decreases and fatty acids are largely converted into triglycerides and stored as an energy reserve in adipose tissue. To investigate the effect of age on growth, a matched set of *S6K1*-deficient (*S6K1*$^{-/-}$) and wild-type male mice were placed on a normal chow diet (NCD) (4% total calories derived from fat, 3,035 kcal kg^{-1}) and monitored over a period of 17 weeks from 10 weeks of age. The rate at which *S6K1*$^{-/-}$ mice increased body weight on the NCD was significantly reduced compared with wild-type mice: at 27 weeks of age the difference in body weight was 25% (Fig. 1a). Dissection of *S6K1*$^{-/-}$ mice revealed a marked reduction in epididymal white adipose tissue (WAT) (Supplementary Fig. 1a). When normalized for body weight, epididymal, inguinal and retroperitoneal fat pads (Fig. 1b), as well as the brown fat pad (Supplementary Fig. 1b) were significantly reduced. Furthermore, the decrease was specific for fat, as the weight of other major organs such as liver was not affected after correction for total body weight (Fig. 1b).

Analysis of adipocytes in epididymal fat pads by either scanning electron microscopy or by haematoxylin and eosin staining showed a sharp reduction in size, with some adipocytes exhibiting a multilocular-like phenotype (Fig. 1c and see below). Morphometric analysis revealed that *S6K1*$^{-/-}$ adipocytes were consistently smaller compared with adipocytes from wild-type mice (Fig. 1c), with an average 71% decrease in size (Supplementary Fig. 1c). The decrease in fat accumulation in *S6K1*$^{-/-}$ mice was not due to less food intake, which was increased 17% when food consumption was adjusted for body weight (Fig. 1d). Moreover, on the basis of normal fasting and feeding glucose levels and no increase in ketone body formation[3] (Table 1), *S6K1*$^{-/-}$ mice did not seem to be starving, nor was there an alteration in adaptive thermogenesis (data not shown). This raised the possibility that triglycerides were being broken down rather than stored in WAT. Consistent with this, basal rates of lipolysis were fivefold higher in *S6K1*$^{-/-}$ versus wild-type adipocytes, although norepinephrine-induced fatty acid and glycerol release increased in both genotypes in a dose-dependent manner to the same final extent (Fig. 1e; see also Supplementary Fig. 1d). Moreover the metabolic rate was greatly enhanced in *S6K1*$^{-/-}$ mice, as indicated by the 27% increase in oxygen consumption versus wild-type mice (Fig. 1f). The respiratory exchange ratio (RER) of 0.713 ± 0.004 for wild-type mice and 0.709 ± 0.003 for *S6K1*$^{-/-}$ mice ($P < 0.01$) showed that both animals were largely using fatty acids as an energy source. Thus the failure to accumulate fat with age in *S6K1*$^{-/-}$ mice seems to stem from a sharp increase in lipolytic and metabolic rates.

These increased responses, combined with the finding that levels of circulating triglycerides and free fatty acids (FFAs) were similar in both genotypes (Table 1), suggested that in *S6K1*$^{-/-}$ mice triglycerides were being rapidly oxidized in WAT and/or muscle. WAT is not an energy-consuming tissue; however, electron micrographs revealed multi-locular adipocytes, with mitochondria of increased size and number—phenotypes that are absent in wild-type adipocytes (Fig. 2a). Consistent with this, analysis of the messenger RNA levels of genes involved in energy combustion and oxidative phosphorylation were found to be strongly increased in *S6K1*$^{-/-}$ adipocytes compared with wild-type adipocytes, including uncoupling protein 1 (UCP1), UCP3, carnitine palmitoyltransferase 1 (CPT1) and PPAR-γ co-activator 1-α (PGC1-α) (Fig. 2a; see also Supplementary Fig. 2a). Mitochondrial content was also affected in *S6K1*$^{-/-}$ skeletal muscle (Fig. 2b), consistent with increased expression of peroxisome proliferator-activated receptor β/δ (PPAR-β/δ), PGC1-α, UCP3 and CPT1 (Fig. 2b; see also Supplementary Fig. 2b). As *S6K1*$^{-/-}$ mice have reduced WAT and increased oxidative phosphorylation, this raised the possibility that *S6K1*$^{-/-}$ mice are protected against diet-induced obesity, which is linked to the oxidative phosphorylation pathway[6–10]. Indeed, when *S6K1*$^{-/-}$ mice were challenged with a high fat diet (HFD) (60% total calories derived from fat, 4,057 kcal kg^{-1}) weight accumulation was significantly reduced compared with wild-type mice during the 4-month feeding period (Figs 2c, d). Although food intake in *S6K1*$^{-/-}$ mice is similar to that of wild-type mice, when normalized to body weight they consume 44% more food (Supplementary Fig. 2c). Metabolic rate measured by indirect calorimetry increased for both genotypes on the HFD, with the effect more pronounced for *S6K1*$^{-/-}$ mice (compare Figs 2e and 1f).

Table 1 **One-hour post-prandial values after overnight fasting of wild-type and *S6K1*$^{-/-}$ mice**

	Wild type		*S6K1*$^{-/-}$	
Diet	Normal	High fat	Normal	High fat
Insulin (μg l^{-1})	0.57 ± 0.09	2.22 ± 0.87	0.38 ± 0.08†	0.27 ± 0.06†
Triglycerides (mmol l^{-1})	0.61 ± 0.09	1.08 ± 0.15	0.55 ± 0.06	0.95 ± 0.14
FFAs (mmol l^{-1})	0.26 ± 0.05	0.27 ± 0.02	0.19 ± 0.04	0.56 ± 0.10†
Leptin (ng ml^{-1})	6.11 ± 0.82	12.6 ± 0.00	3.22 ± 0.50	6.34 ± 2.35†
β-Hydroxybutyrate (mg dl^{-1})*	1.30 ± 0.05	ND	1.40 ± 0.16	ND

Values are for 6-month-old male mice of the indicated genotype fed a normal or high fat diet. Data represent mean ± s.e.m. ND, not determined.
*The level of β-hydroxybutyrate was measured in 6-h-fasted mice.
†$P < 0.05$ compared with wild type ($n = 6$–18).

Moreover RER remained unchanged in *S6K1* $^{-/-}$ mice on a HFD (0.708 ± 0.002), whereas in wild-type mice it increased from 0.713 ± 0.004 to 0.729 ± 0.002 ($n = 6$, $P < 0.01$), indicating an increase in carbohydrate relative to fatty acid oxidation. To determine the weight gain corresponding to fat, mice were subjected to magnetic resonance imaging (MRI) analysis at 2-month intervals while on the HFD. A transverse section through the abdomen showed a marked reduction in fat depots, depicted by the less intense signal (Supplementary Fig. 2d). MRI assessment of total fat, corrected for body weight, revealed that the body fat index for *S6K1* $^{-/-}$ mice increased by 20% over this period, whereas it doubled for wild-type mice (Fig. 2f). Thus, consistent with the increase in oxidative phosphorylation, *S6K1* $^{-/-}$ mice are protected against diet-induced obesity.

Although *S6K1* $^{-/-}$ mice have a high metabolic rate when on a HFD, they exhibit a threefold increase in circulating FFAs (Table 1), consistent with an increase in fat on their skin and hair (data not shown). As increased circulating FFAs are implicated in insulin resistance[11–13] and *S6K1* $^{-/-}$ mice are hypoinsulinaemic[3], it seemed likely that they would become insulin resistant on the HFD. On a NCD both *S6K1* $^{-/-}$ and wild-type mice exhibited similar fasting levels of glucose (Fig. 3a), although *S6K1* $^{-/-}$ mice were more insulin sensitive, as indicated by faster glucose clearance in the insulin tolerance test (Fig. 3a). In contrast, both genotypes displayed increased hyperglycaemia on a HFD, although the effect was more pronounced in wild-type mice (Fig. 3b). However, despite the increases in glucose and in FFAs, *S6K1* $^{-/-}$ mice remain as insulin sensitive on a HFD as on a NCD (Fig. 3b versus a). In the case of wild-type mice, insulin resistance on a HFD (Fig. 3b) can be explained by persistently elevated insulin levels (Table 1), inducing insulin receptor desensitization, as measured by reduced receptor auto-phosphorylation in response to insulin (Fig. 3c). In *S6K1* $^{-/-}$ mice insulin levels fail to rise on a HFD (Table 1), consistent with higher insulin receptor auto-phosphorylation (Fig. 3c). However, insulin receptors still desensitize in *S6K1* $^{-/-}$ mice on a HFD (Fig. 3c), probably due to the large increase in FFA levels (Table 1). That insulin receptors desensitize in *S6K1* $^{-/-}$ mice but remain insulin sensitive suggests that absence of S6K1 facilitates insulin signalling downstream of the insulin receptor. To test this we monitored protein kinase B (PKB) phosphorylation, as insulin sensitivity is tightly linked to the phosphatidylinositol-3-OH kinase (PI(3)K)–PKB signalling pathway[14]. As with insulin receptor auto-phosphorylation in wild-type mice on a HFD, insulin-induced PKB phosphorylation was suppressed in fat, liver and muscle compared with wild-type mice maintained on a NCD (Fig. 3d). However, there was no significant effect on PKB phosphorylation in *S6K1* $^{-/-}$ mice,

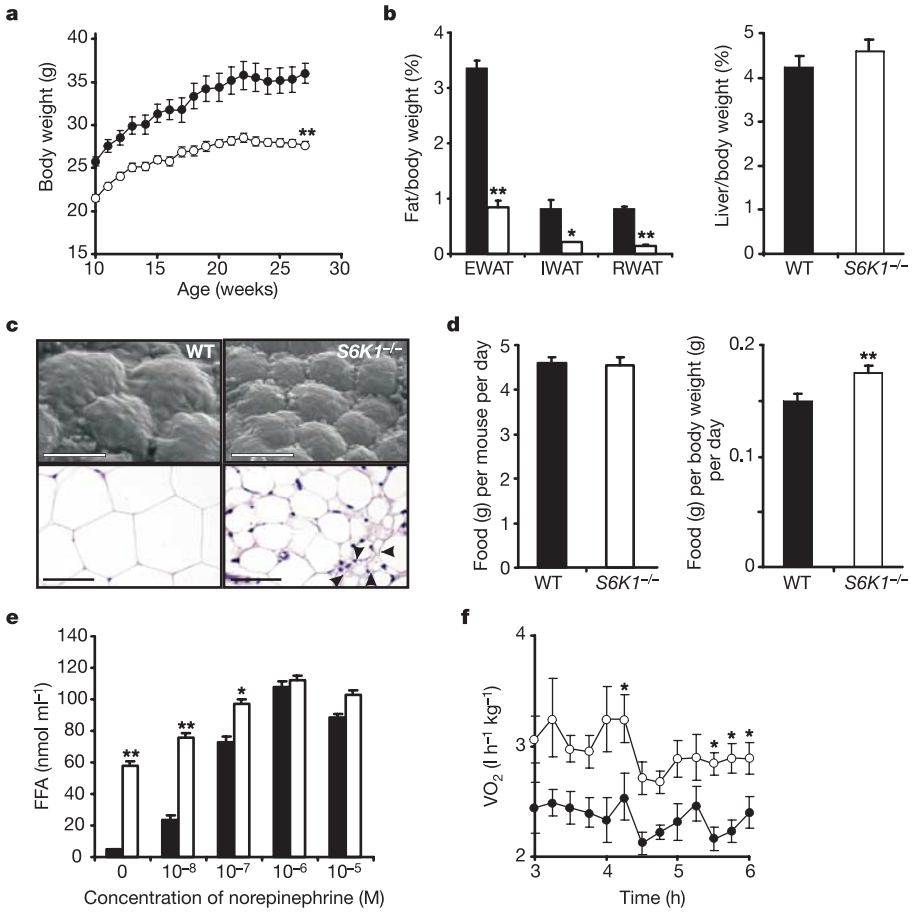

Figure 1 Reduced adiposity in *S6K1* $^{-/-}$ mice. **a**, Growth curves of wild-type and *S6K1* $^{-/-}$ mice on a NCD. Wild type, $n = 11$; *S6K1* $^{-/-}$, $n = 13$. **b**, Weights of epididymal, inguinal and retroperitoneal adipose tissue (EWAT, IWAT and RWAT, respectively) and liver normalized by body weight ($n = 6$ each genotype). WT, wild type. **c**, Scanning electron microscopic (top) and histological analysis of epididymal WAT (bottom). Arrowheads indicate multi-locular adipocytes. Magnification for scanning microscopy and for histology are × 500 and × 200, respectively. Mice were 6-month-old males in **b** and **c**. **d**, Food intake per mouse measured over 15 days ($n = 12$; $P = 0.8$) or normalized by body weight ($n = 12$). **e**, Enhanced lipolysis in *S6K1* $^{-/-}$ adipocytes. **f**, Oxygen consumption (VO_2) in wild-type and *S6K1* $^{-/-}$ mice fed a NCD ($n = 6$ each genotype). All values are given as mean ± s.e.m. Asterisk, $P < 0.01$; double asterisk, $P < 0.001$. Filled symbols/columns indicate wild type; open symbols/columns, *S6K1* $^{-/-}$ mice.

regardless of diet or tissue (Fig. 3d). This suggested that S6K1 elicited a selective inhibitory effect on PKB activation at a point downstream of the insulin receptor, consistent with little effect on mitogen activated protein kinase and S6K1 activation in wild-type animals on a HFD (see below and data not shown).

Recently, we demonstrated in *Drosophila* that dS6K negatively regulates dPKB activity in a cell-autonomous manner[15]. To test whether this was the mechanism responsible for the observed responses, S6K1 levels were reduced with small interfering RNAs. The results show that lowering S6K1 levels potentiates insulin-induced PKB phosphorylation, with no effect on insulin receptor auto-phosphorylation (Fig. 3e), suggesting that the target of inhibition resided downstream of the insulin receptor. Indeed, reduction of S6K1 levels is paralleled by a decrease in phosphorylation of S307 and S636/S639 of insulin receptor substrate 1 (IRS1) (Fig. 3e), sites shown to inhibit PI(3)K binding to IRS1 (ref. 4) and

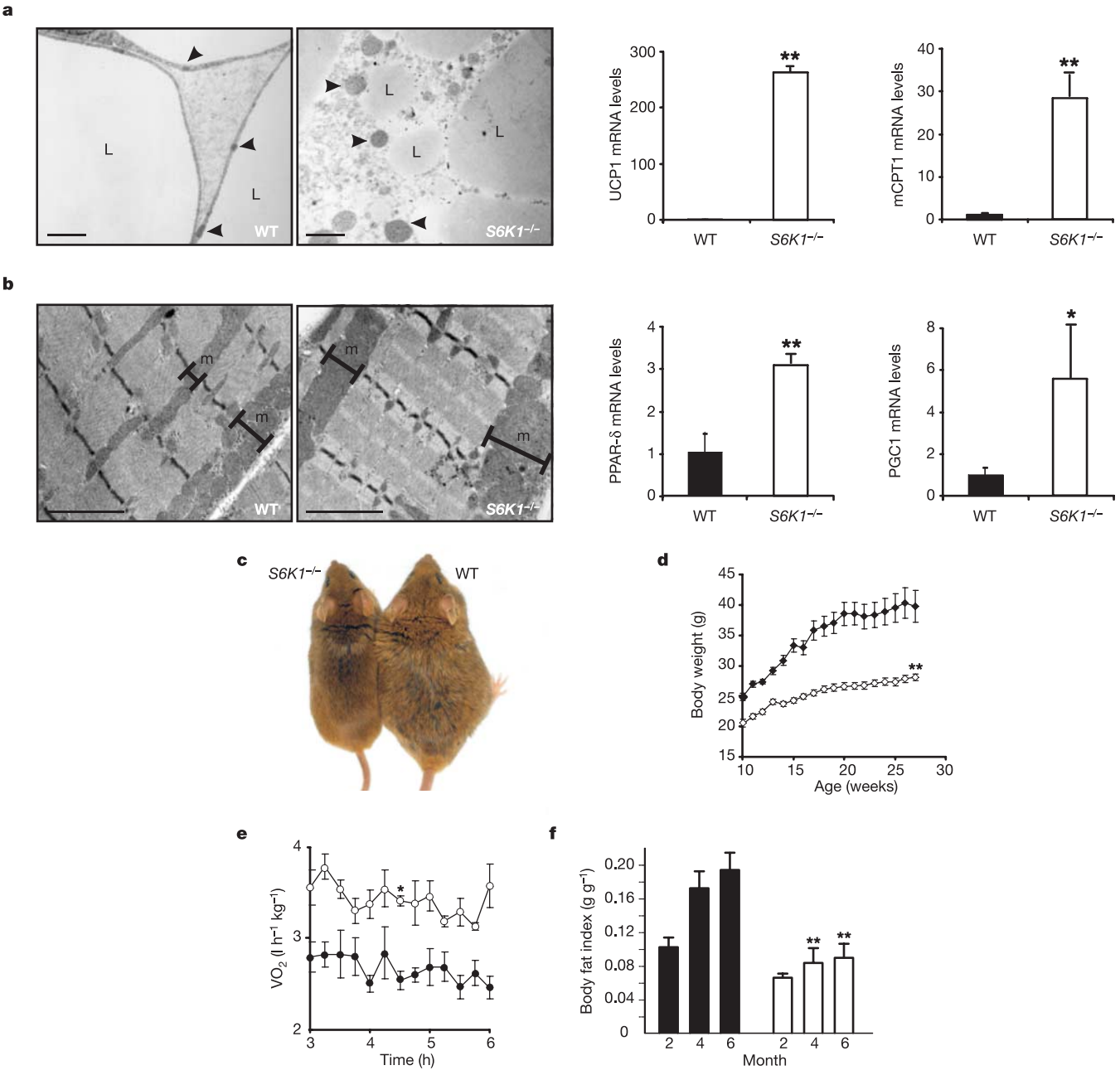

Figure 2 Increased mitochondria and resistance to diet-induced obesity. **a**, The left panels show transmission electron microscopic analysis of epididymal fat. Arrowheads indicate mitochondria and lipid droplets (L) (× 5,000 magnification). The right panels show UCP1 and mCPT1 mRNA (relative values) measured by quantitative RT–PCR (see Methods). **b**, The left panels show transmission electron microscopic analysis of plantaris muscle (× 10,000 magnification). m, mitochondria. The right panels show PPAR-δ and PGC1 mRNA levels (relative values) measured by quantitative RT–PCR. In **a**, **b**, $n = 4$–7; asterisk, $P < 0.01$; double asterisk, $P < 0.001$. **c**, Representative wild-type and *S6K1* $^{-/-}$ mice after 6 months feeding on a HFD. **d**, Growth curves of wild-type and *S6K1* $^{-/-}$ mice maintained on a HFD. WT, $n = 11$; *S6K1* $^{-/-}$, $n = 15$; $P < 0.001$. **e**, Oxygen consumption (VO_2) in wild-type and *S6K1* $^{-/-}$ mice maintained on a HFD for 6 months ($n = 6$ each genotype). **f**, Body fat index determined by MRI analysis of wild-type ($n = 10$) and *S6K1* $^{-/-}$ mice ($n = 12$) maintained on a HFD for 4 months. Filled symbols/columns indicate wild type; open symbols/columns, *S6K1* $^{-/-}$ mice. Values are mean ± s.e.m. Asterisk, $P < 0.01$; double asterisk, $P < 0.001$ in **d**–**f**.

to be involved in insulin resistance in skeletal muscle cells from patients with type 2 diabetes[5]. Thus, removal of S6K1 can facilitate insulin signalling in a cell-autonomous manner.

Hyperglycaemia, hyperaminoacidaemia and hyperlipidaemia are associated with obesity and insulin resistance[16]; however, the role of increased nutrients in insulin action is not well understood[17–19]. As S6K1 is activated by nutrients[20–22] and acts negatively on PI(3)K signalling, this raised the possibility that on a HFD S6K1 is involved in inducing insulin resistance. This hypothesis is supported by the reversal of amino acid inhibition of insulin-induced PI(3)K signalling by rapamycin, which inhibits mTOR[23], an immediate upstream S6K1 kinase[2]. Consistent with this hypothesis, phosphorylation of S6K1 T389, S6 S240/S244, IRS1 S307 and IRS1 S636/S639 is highly elevated in wild-type mice maintained on a HFD compared with wild-type mice maintained on a NCD (Fig. 4a, b). Furthermore, the increase in IRS1 S307 and S636/S639 phosphorylation is absent in *S6K1*$^{-/-}$ mice on a HFD (Fig. 4b). Under these conditions there were no apparent alterations in IRS1 levels (Fig. 4b). These findings suggest that nutrient-induced S6K1 activation acts to suppress insulin signalling through modulating IRS1 S307 and S636/S639 phosphorylation. To test this further, two genetic models of obesity were examined: *K/K A*^{y} and *ob/ob* mice[24,25]. The results show that the *K/K A*^{y} and *ob/ob* mice maintained on a NCD have elevated S6K1 T389, S6 S240/S244, IRS1 S307 and IRS1 S636/S639 phosphorylation as compared with wild-type mice on a NCD (Fig. 4c). Moreover, in contrast with PKB S473 phosphorylation in adipose and muscle (Fig. 3d), insulin stimulates S6K1 T389 phosphorylation to even higher levels in wild-type animals on a HFD compared with a NCD (Fig. 4d), potentially further suppressing PI(3)K signalling. Thus, either nutritionally or genetically driven obesity leads to the upregulation of S6K1, which may in turn act to suppress PI(3)K signalling, contributing to insulin resistance.

The results presented here indicate that *S6K1*$^{-/-}$ mice are protected against obesity and insulin resistance due to the upregulation of the oxidative phosphorylation pathway and increased insulin sensitivity. Enhanced oxidative metabolism is consistent with the increase in mitochondria number, as well as the induction of genes that control the oxidative phosphorylation pathway. That *S6K1*$^{-/-}$ mice remain insulin sensitive despite high circulating FFAs may be explained by the strong protection against metabolic syndrome by overexpression or activation of PPAR-δ[6–8]. Despite the increase in the oxidative phosphorylation pathway and reduced insulin levels, circulating glucose and FFA levels still rise in *S6K1*$^{-/-}$ mice; however, these animals remain sensitive to insulin, and PI(3)K

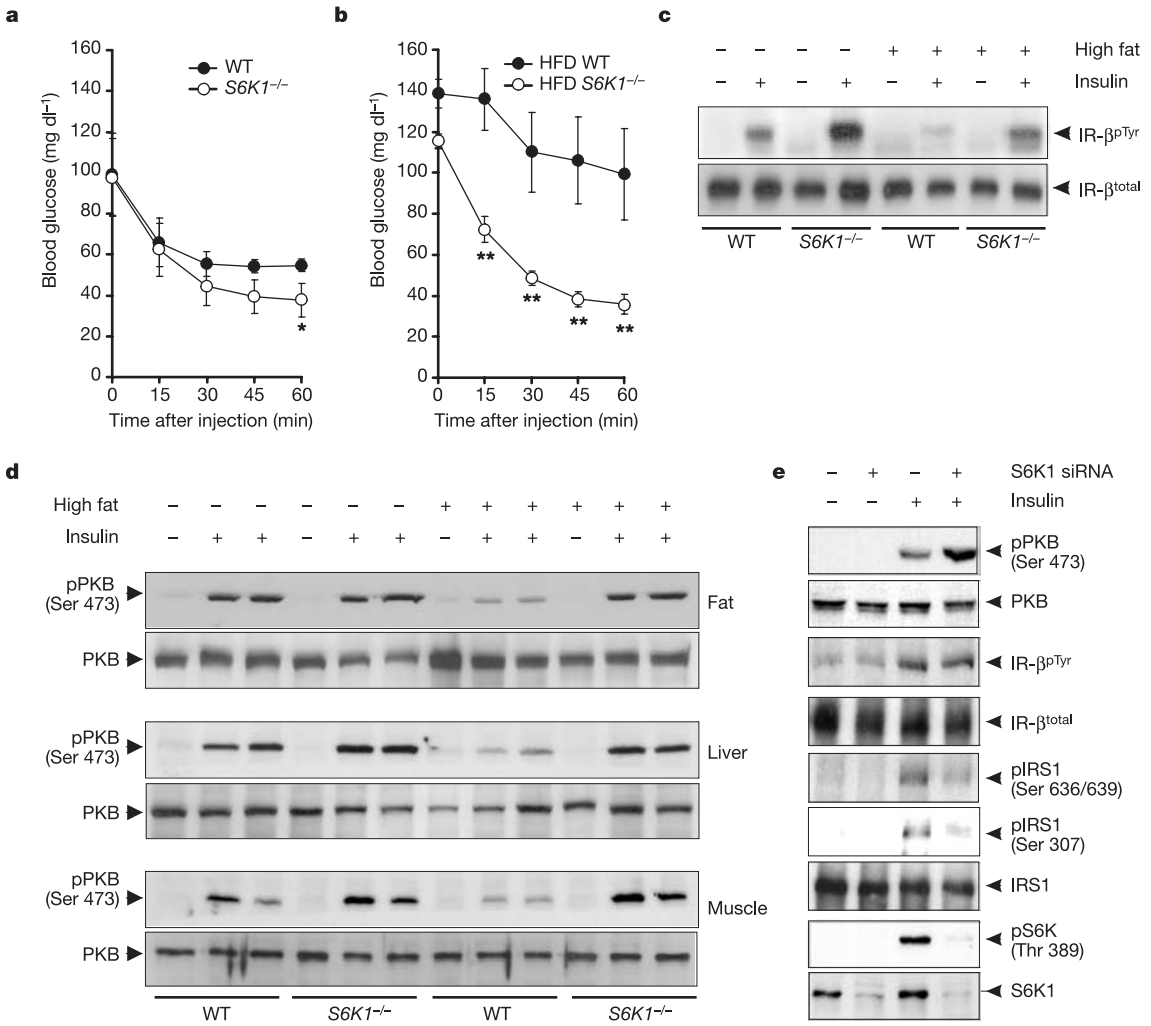

Figure 3 Enhanced insulin sensitivity and insulin signalling in the absence of S6K1. **a**, **b**, Insulin tolerance test in 3-h-fasted mice on a NCD (**a**) or HFD (**b**) at 6 months of age. Asterisk, $P < 0.05$; double asterisk, $P < 0.01$. Values are mean ± s.e.m. **c**, Insulin receptor tyrosine phosphorylation in liver of wild-type and *S6K1*$^{-/-}$ mice before (−) or after (+) insulin stimulation on a NCD or HFD. **d**, Level of phosphorylation of PKB Ser 473 in fat, liver and muscle ($n = 3$–8 for each genotype in **c**, **d**). **e**, Lowering S6K1 expression by siRNA potentiates insulin-induced PKB phosphorylation in HeLa cells.

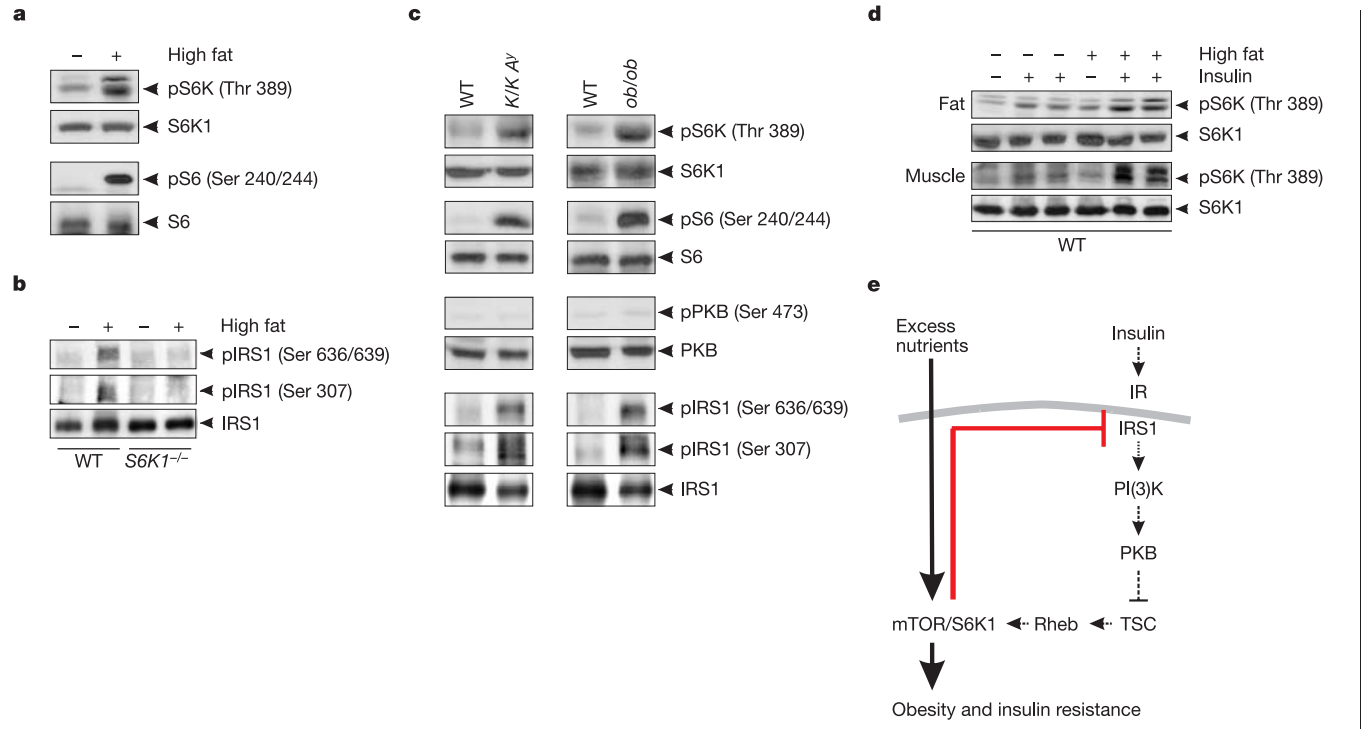

Figure 4 S6K1 activation in obesity. **a**, S6K1 Thr 389 and S6 Ser 240/244 phosphorylation in fat of wild-type mice maintained on a NCD (−) or HFD (+) for 4 months. **b**, IRS1 Ser 307 and Ser 636/639 phosphorylation in fat of wild-type or *S6K1* $^{-/-}$ mice maintained on a NCD (−) or HFD (+). **c**, S6K1 Thr 389, S6 Ser 240/244, IRS1 Ser 307 and IRS1 Ser 636/639 phosphorylation in fat of wild-type, *K/K A*^{y} or *ob/ob* mice maintained on a NCD. **d**, S6K1 Thr 389 phosphorylation in fat or muscle of wild-type mice maintained on a NCD or HFD for 4 months before (−) or after (+) injection of insulin (0.75 U kg^{-1} of body weight). All mice of each genotype (n = 3–8) in **a**–**d** were fasted for 6 h and were 6 months old. **e**, Model of inhibition of IRS1 signalling through activation of S6K1.

signalling is unaffected. This observation may be explained by the loss of S6K1, whose activation by either nutrients or insulin leads to increased IRS1 serine phosphorylation (Fig. 4e). In the case of insulin, this is mediated by a negative feedback loop triggered by PKB phosphorylation of the TSC1/2 tumour suppressor complex, leading to Rheb activation and stimulation of S6K1 (ref. 26). Thus, in a homeostatic setting, as nutrients and amino acids are consumed, mTOR/S6K1 activity would decrease, restoring PI(3)K signalling, whereas the incessant supply of nutrients associated with the obese state would lead to constitutive activation of mTOR/S6K1 and desensitization of insulin signalling (Fig. 4e). Taken together the results suggest that S6K1 may have a central function along with other signalling components in development of obesity and insulin resistance, and may be an important drug target in the treatment of patients suffering from these pathological disorders. □

Methods

Mice

S6K1 $^{-/-}$ mice were generated as previously described[3]. Male C57BL/6J, *K/K A*^{y} and *ob/ob* (C57BL/6J background) mice were obtained from E. Janvier, CLEA Japan Inc., and The Jackson Laboratory, respectively.

Metabolic studies

At 10 weeks of age male mice were placed on either a NCD (diet number 3807, KLIBA-NAFAG) or HFD *ad libitum* (diet D12492, Researchdiets) and monitored for 24 weeks. Body weight was recorded weekly and food intake was measured every second day for 15 consecutive days. Insulin tolerance tests, oxygen consumption, RER measurements and quantification of blood metabolites were performed as previously described[27].

Histology and morphometric analysis of tissues

Adipose tissue was analysed by haematoxylin and eosin staining as previously described[27]. Morphometric analysis of epididymal WAT from 500 or more cells from three different animals per genotype was performed with ImageJ software (NIH). Adipose and plantaris muscle tissue were prepared as described for scanning and transmission electron microscopy[27].

Magnetic resonance imaging analysis

MRI experiments were carried out on a Biospec 47/30 spectrometer (Bruker Medical) at 4.7 T equipped with a self-shielded 12-cm bore gradient system[28]. Animals were anaesthetized with 1.5% isoflurane (Abbott). Adipose tissue was measured with an optimized turbo-RARE2 imaging sequence. Acquisition parameters were: repetition delay (TR) = 250 ms; echo delay (TE) = 8.6 ms; RARE factor = 32 (effective echo time 73.1 ms); number of averages = 8; slice orientation transverse, image matrix = 128 × 128 pixels; field-of-view = 3.5 × 3.5 cm; slice thickness = 1.2 mm (contiguous). Fat pad volumes were assessed with an in-house software algorithm based on IDL software package (Research Systems Inc.). Body fat indices were calculated by dividing adipose tissue weight by body weight.

Lipolysis in isolated adipocytes

Primary adipocytes were prepared from epididymal fat pads as described previously[29]. Cells were incubated for 30 min at 37 °C with or without norepinephrine (Sigma-Aldrich SARL) at the indicated concentrations.

Real-time quantitative RT–PCR

Total RNA was extracted from frozen tissue samples or cells using the RNeasy kit (Qiagen). Complementary DNA was synthesized from total RNA with the SuperScript First-Strand Synthesis System (Invitrogen) and random hexamer primers. The real-time polymerase chain reaction (PCR) measurement of individual cDNAs was performed using SYBR green dye to measure duplex DNA formation with the Roche Lightcycler system and normalized to the expression of either β-actin or 18S ribosomal RNA. The primers and probes used in the real time RT–PCR were the following: UCP1 sense 5′-GGCCCTTGT AAACAACAAAATAC-3′, antisense 5′-GGCAACAAGAGCTGACAGTAAAT-3′; UCP3 sense 5′-ACTCCAGCGTCGCCATCAGGATTCT-3′, antisense 5′-TAAACAGGTGAG ACTCCAGCAACTT-3′; mCPT1 sense 5′-TTGCCCTACAGCTCTGGCATTTCC-3′, antisense 5′-GCACCCAGATGATTGGGATACTGT-3′; mPPAR-δ sense 5′-CTCTTCATC GCGGCCATCATTCT-3′, antisense 5′-TCTGCCATCTTCTGCAGCAGCTT-3′; PGC-1 sense 5′-AAGTGTGGAACTCTCTGGAACTG-3′, antisense 5′-GGGTTATCTTGGTTGG CTTTATG-3′.

Measurement of insulin receptor and IRS1 phosphorylation *in vivo*

After a 6-h fast mice were injected intravenously with 0.75 U kg^{-1} insulin (Eli Lilly) or equal volume of vehicle. All indicted tissues were collected in liquid nitrogen 5 min after injection. Protein extracts from tissue samples were analysed as described[30]. Antibodies were from Santa Cruz (anti-insulin receptor β and anti-S6K1 antibodies), Upstate Biotechnology (anti-phosphotyrosine and anti-IRS1 antibodies) and Cell Signaling (anti-PKB, anti-phospho-PKB Ser 473, anti-phospho-IRS1 Ser 636/639, anti-phospho-S6K Thr 389 and anti-phospho-S6 240/244 antibodies). Antibodies to S6 and phospho-IRS1 Ser 307 were from J. Mestan and Y. Le Marchand-Brustel, respectively.

RNA interference

RNA interference (RNAi) duplexes corresponding to human S6K1 (5′-AAGGGGGCTATGGAAAGGTTT-3′) were purified, annealed and transfected into HeLa cells using oligofectamine (Invitrogen). After 60 h cells were deprived of serum overnight and either lysed directly or stimulated with 200 nM insulin for 30 min. The effect of RNAi on S6K1 expression and PKB phosphorylation was measured by western blot analysis. Cell lysates were incubated for 4 h with anti-IRS1 or anti-insulin receptor β antibody pre-absorbed on protein A Sepharose at 4 °C, and analysed by western blot analyses after gel electrophoresis.

Statistical analysis

Data are presented as mean ± s.e.m. The main and interactive effects were analysed by analysis of variance (ANOVA) factorial, repeated measurements or by one-way ANOVA followed by Bonferroni *t*-test (MRI analysis). Differences between individual group means were analysed by Fisher's PLSD test. Analyses were performed using Statview Software (Brainpower).

Received 19 April; accepted 21 July 2004; doi:10.1038/nature02866.
Published online 11 August 2004.

1. Saltiel, A. R. & Kahn, C. R. Insulin signalling and the regulation of glucose and lipid metabolism. *Nature* **414,** 799–806 (2001).
2. Fingar, D. C., Salama, S., Tsou, C., Harlow, E. & Blenis, J. Mammalian cell size is controlled by mTOR and its downstream targets S6K1 and 4EBP1/eIF4E. *Genes Dev.* **16,** 1472–1487 (2002).
3. Pende, M. *et al.* Hypoinsulinaemia, glucose intolerance and diminished β-cell size in S6K1-deficient mice. *Nature* **408,** 994–997 (2000).
4. Zick, Y. Insulin resistance: a phosphorylation-based uncoupling of insulin signaling. *Trends Cell Biol.* **11,** 437–441 (2001).
5. Bouzakri, K. *et al.* Reduced activation of phosphatidylinositol-3 kinase and increased serine 636 phosphorylation of insulin receptor substrate-1 in primary culture of skeletal muscle cells from patients with type 2 diabetes. *Diabetes* **52,** 1319–1325 (2003).
6. Tanaka, T. *et al.* Activation of peroxisome proliferator-activated receptor delta induces fatty acid β-oxidation in skeletal muscle and attenuates metabolic syndrome. *Proc. Natl Acad. Sci. USA* **100,** 15924–15929 (2003).
7. Luquet, S. *et al.* Peroxisome proliferator-activated receptor delta controls muscle development and oxidative capability. *FASEB J.* **17,** 2299–2301 (2003).
8. Dressel, U. *et al.* The peroxisome proliferator-activated receptor beta/delta agonist, GW501516, regulates the expression of genes involved in lipid catabolism and energy uncoupling in skeletal muscle cells. *Mol. Endocrinol.* **17,** 2477–2493 (2003).
9. Patti, M. E. *et al.* Coordinated reduction of genes of oxidative metabolism in humans with insulin resistance and diabetes: Potential role of PGC1 and NRF1. *Proc. Natl Acad. Sci. USA* **100,** 8466–8471 (2003).
10. Mootha, V. K. *et al.* PGC-1α-responsive genes involved in oxidative phosphorylation are coordinately downregulated in human diabetes. *Nature Genet.* **34,** 267–273 (2003).
11. Boden, G. Role of fatty acids in the pathogenesis of insulin resistance and NIDDM. *Diabetes* **46,** 3–10 (1997).
12. Kahn, B. B. Type 2 diabetes: when insulin secretion fails to compensate for insulin resistance. *Cell* **92,** 593–596 (1998).
13. Le Marchand-Brustel, Y. *et al.* Fatty acid-induced insulin resistance: role of insulin receptor substrate 1 serine phosphorylation in the retroregulation of insulin signalling. *Biochem. Soc. Trans.* **31,** 1152–1156 (2003).
14. Jiang, G. & Zhang, B. B. Pi 3-kinase and its up- and down-stream modulators as potential targets for the treatment of type II diabetes. *Front. Biosci.* **7,** d903–d907 (2002).
15. Radimerski, T., Montagne, J., Hemmings-Mieszczak, M. & Thomas, G. Lethality of *Drosophila* lacking TSC tumor suppressor function rescued by reducing dS6K signaling. *Genes Dev.* **16,** 2627–2632 (2002).
16. Kahn, B. B. & Flier, J. S. Obesity and insulin resistance. *J. Clin. Invest.* **106,** 473–481 (2000).
17. Proietto, J., Filippis, A., Nakhla, C. & Clark, S. Nutrient-induced insulin resistance. *Mol. Cell. Endocrinol.* **151,** 143–149 (1999).
18. Greiwe, J. S., Kwon, G., McDaniel, M. L. & Semenkovich, C. F. Leucine and insulin activate p70 S6 kinase through different pathways in human skeletal muscle. *Am. J. Physiol. Endocrinol. Metab.* **281,** E466–E471 (2001).
19. Patti, M. E. Nutrient modulation of cellular insulin action. *Ann. NY Acad. Sci.* **892,** 187–203 (1999).
20. Hara, K. *et al.* Amino acid sufficiency and mTOR regulate p70 S6 kinase and eIF-4E BP1 through a common effector mechanism. *J. Biol. Chem.* **273,** 14484–14494 (1998).
21. Patti, M. E., Brambilla, E., Luzi, L., Landaker, E. J. & Kahn, C. R. Bidirectional modulation of insulin action by amino acids. *J. Clin. Invest.* **101,** 1519–1529 (1998).
22. Dennis, P. B. *et al.* Mammalian TOR: a homeostatic ATP sensor. *Science* **294,** 1102–1105 (2001).
23. Tremblay, F. & Marette, A. Amino acid and insulin signaling via the mTOR/p70 S6 kinase pathway. A negative feedback mechanism leading to insulin resistance in skeletal muscle cells. *J. Biol. Chem.* **276,** 38052–38060 (2001).
24. Iwatsuka, H., Shino, A. & Suzuoki, Z. General survey of diabetic features of yellow KK mice. *Endocrinol. Jpn* **17,** 23–35 (1970).
25. Zhang, Y. *et al.* Positional cloning of the mouse obese gene and its human homologue. *Nature* **372,** 425–432 (1994).
26. Manning, B. D. & Cantley, L. C. Rheb fills a GAP between TSC and TOR. *Trends Biochem. Sci.* **28,** 573–576 (2003).
27. Picard, F. *et al.* SRC-1 and TIF2 control energy balance between white and brown adipose tissues. *Cell* **111,** 931–941 (2002).
28. Doty, F. D., Entzminger, G. Jr, Hauck, C. D. & Staab, J. P. Practical aspects of birdcage coils. *J. Magn. Reson.* **138,** 144–154 (1999).
29. Marette, A., Tulp, O. L. & Bukowiecki, L. J. Mechanism linking insulin resistance to defective thermogenesis in brown adipose tissue of obese diabetic SHR/N-cp rats. *Int. J. Obes.* **15,** 823–831 (1991).
30. Hirosumi, J. *et al.* A central role for JNK in obesity and insulin resistance. *Nature* **420,** 333–336 (2002).

Supplementary Information accompanies the paper on **www.nature.com/nature**.

Acknowledgements We thank T. Opgenorth and C. Rondinone for sharing their results before publication; G. S. Hotamisligil, S. Y. Kim and D. J. Withers for their critical reading of the manuscript; and S. Cinti, P. B. Dennis, A. Dulloo, L. Fajas, A. Greenberg, B. M. Spiegelman, G. Solinas, J. Tanti and M. Wymann for discussions. We are also grateful to M.-F. Champy, W. Theilkaes, N. Messaddeq, I. Obergfoell and J. F. Spetz for the blood analysis, studies with MRI, technical assistance with electron microscopy, for photography and for assistance in the animal experiments, respectively. Work in the laboratory of J.A. is supported by grants from CNRS, INSERM, ULP, Hôpital Universitaire de Strasbourg, NIH, EMBO and the European community, and the laboratory of S.C.K. and G.T. is supported by the Novartis Institutes for Biomedical Research and a grant from the Swiss Cancer League.

Competing interests statement The authors declare that they have no competing financial interests.

Correspondence and requests for materials should be addressed to G.T. (gthomas@fmi.ch).

Cytoplasmic PML function in TGF-β signalling

Hui-Kuan Lin, Stephan Bergmann & Pier Paolo Pandolfi

Cancer Biology and Genetics Program, Department of Pathology, Memorial Sloan-Kettering Cancer Center, Sloan-Kettering Institute, 1275 York Avenue, New York, New York, 10021, USA

Transforming growth factor β (TGF-β) is a pluripotent cytokine that controls key tumour suppressive functions[1–3], but cancer cells are often unresponsive to it[1,4]. The promyelocytic leukaemia (PML) tumour suppressor of acute promyelocytic leukaemia (APL) accumulates in the PML nuclear body, but cytoplasmic PML isoforms of unknown function have also been described[5,6]. Here we show that cytoplasmic *Pml* is an essential modulator of TGF-β signalling. *Pml*-null primary cells are resistant to TGF-β-dependent growth arrest, induction of cellular senescence and apoptosis. These cells also have impaired phosphorylation and nuclear translocation of the TGF-β signalling proteins Smad2 and Smad3, as well as impaired induction of TGF-β target genes. Expression of cytoplasmic *Pml* is induced by TGF-β. Furthermore, cytoplasmic PML physically interacts with Smad2/3 and SARA (Smad anchor for receptor activation) and is required for association of Smad2/3 with SARA and for the accumulation of SARA and TGF-β receptor in the early endosome. The PML–RARα oncoprotein of APL can antagonize cytoplasmic PML function and APL cells have defects in TGF-β signalling similar to those observed in *Pml*-null cells. Our findings identify cytoplasmic PML as a critical TGF-β regulator, and further implicate deregulated TGF-β signalling in cancer pathogenesis.

APL is almost invariably associated with chromosomal translocations involving the *PML* tumour suppressor and *RARα* genes, resulting in the generation of a PML–RARα leukaemogenic fusion protein that can function as a dominant-negative PML and RARα mutant[7–9]. PML–RARα physically interacts with nuclear PML isoforms causing their delocalization from the PML nuclear body (PML-NB) into aberrant microspeckled nuclear structures[7,8]. Until

additional model whereby natural restriction factors may act by preventing capsid disassembly. In turn, compounds that cross-link capsid components, such as multi-functional reagents designed to target the central channel of the hexamer, might be expected to inhibit retroviral replication. □

Methods

Protein production

The DNA sequence coding for the NTD of N-MLV (capsid residues Pro 1 to Ser 132) was amplified by polymerase chain reaction (PCR) using a plasmid containing the proviral DNA[26] as a template. The PCR product was inserted into a pET22b expression vector (Novagen) between the *Nde*I and *Xho*I restriction sites in order to produce a C-terminal hexa-histidine fusion and the sequence Met-Pro at the N terminus. The protein was expressed in the *Escherichia coli* strain BL21 (DE3) and purified using ion exchange, immobilized metal ion affinity and gel filtration chromatography. Verification of the processing of the N-terminal methionine to produce the mature form of the protein was analysed by electrospray ionization mass spectrometry (ESI-MS). The double substitution mutant L4M L126M was prepared using the Quickchange site-directed mutagenesis kit (Stratagene). Seleno-methionine-substituted protein was prepared by expressing the protein in the *E. coli* methionine auxotroph B834 (DE3) grown on seleno-methionine-substituted media.

Crystallization and structure solution

Proteins were crystallized using the vapour batch method. A 16–22 mg ml^{-1} solution of N-MLV(NTD) or N-MLV(NTD/L4M L126M) in 150 mM NaCl, 20 mM Tris-HCl pH 8.0 was mixed with an equal volume of crystallization solution containing 13–16% PEG 3350, 100 mM sodium citrate pH 5.6. Two-microlitre droplets were dispensed into 96-well vapour batch plates (Douglas instruments) covered with 6 ml of 'Al's oil' (Hampton Research) using an IMPAX 1-5 robot (Douglas instruments). A solution of 10% (v/v) aqueous isopropanol was placed in the side wells of the tray and the drops equilibrated overnight. Next day, the 10% isopropanol solution was replaced with a 20% (v/v) isopropanol solution and crystals typically grew to $0.2 \times 0.2 \times 0.1$ mm^3 in one to two weeks. Crystals were collected by transfer into fresh crystallization solution supplemented with 10% (v/v) isopropanol and 15% (v/v) 1,2-propanediol as a cryoprotectant then flash-frozen in liquid nitrogen. The crystals belong to the space group $P2_1$ ($a = 86.0$ Å, $b = 78.3$ Å, $c = 85.76$ Å, $\beta = 118.9°$) with six capsid NTDs in the asymmetric unit. The structure was solved by a three-wavelength MAD experiment using seleno-methionine-containing crystals of the double-methionine-substituted N-MLV(NTD/L4M L126M) on Station 14.2 at the Synchrotron Radiation Source (SRS), Daresbury, UK. All data sets were reduced using the HKL suite of processing software. Twelve selenium atoms were located and the phases refined using the program SOLVE[28], resulting in an overall figure of merit (FoM) of 0.61. The local six-fold operators were identified using information from a self-rotation function and the six pairs of Se sites, and were used for averaging and density modification in DM[29]. The quality of this initial map was good enough to build a polyalanine model into a single monomer using the program O. The hexamer was generated by application of the non-crystallographic symmetry operators to the monomer and the fit improved using real-space rigid-body refinement in the program O. Further refinement against a high-resolution data set collected on the SeMet crystal using REFMAC and ARPP[30] resulted in a map into which an essentially complete model was built. The data collection, phasing and refinement statistics are reported in Table 1.

Received 7 July; accepted 5 August 2004; doi:10.1038/nature02915.

1. Swanstrom, R. & Wills, J. W. in *Synthesis, Assembly and Processing of Viral Proteins* (eds Coffin, J. M., Hughes, S. H. & Varmus, H. E.) (Cold Spring Harbor Laboratory Press, New York, 1997).
2. Briggs, J. A., Wilk, T., Welker, R., Krausslich, H. G. & Fuller, S. D. Structural organization of authentic, mature HIV-1 virions and cores. *EMBO J.* **22,** 1707–1715 (2003).
3. Nermut, M. V. & Hockley, D. J. Comparative morphology and structural classification of retroviruses. *Curr. Top. Microbiol. Immunol.* **214,** 1–24 (1996).
4. Li, S., Hill, C. P., Sundquist, W. I. & Finch, J. T. Image reconstructions of helical assemblies of the HIV-1 CA protein. *Nature* **407,** 409–413 (2000).
5. Ganser, B. K., Cheng, A., Sundquist, W. I. & Yeager, M. Three-dimensional structure of the M-MuLV CA protein on a lipid monolayer: a general model for retroviral capsid assembly. *EMBO J.* **22,** 2886–2892 (2003).
6. Kingston, R. L. *et al.* Structure and self-association of the Rous sarcoma virus capsid protein. *Struct. Fold. Des.* **8,** 617–628 (2000).
7. Cornilescu, C. C., Bouamr, F., Yao, X., Carter, C. & Tjandra, N. Structural analysis of the N-terminal domain of the human T-cell leukemia virus capsid protein. *J. Mol. Biol.* **306,** 783–797 (2001).
8. Gamble, T. R. *et al.* Crystal structure of human cyclophilin A bound to the amino-terminal domain of HIV-1 capsid. *Cell* **87,** 1285–1294 (1996).
9. Gitti, R. K. *et al.* Structure of the amino-terminal core domain of the HIV-1 capsid protein. *Science* **273,** 231–235 (1996).
10. Jin, Z., Jin, L., Peterson, D. L. & Lawson, C. L. Model for lentivirus capsid core assembly based on crystal dimers of EIAV p26. *J. Mol. Biol.* **286,** 83–93 (1999).
11. Khorasanizadeh, S., Campos-Olivas, R. & Summers, M. F. Solution structure of the capsid protein from the human T-cell leukemia virus type-I. *J. Mol. Biol.* **291,** 491–505 (1999).
12. Nandhagopal, N. *et al.* Dimeric Rous sarcoma virus capsid protein structure relevant to immature Gag assembly. *J. Mol. Biol.* **335,** 275–282 (2004).
13. Tang, C., Ndassa, Y. & Summers, M. F. Structure of the N-terminal 283-residue fragment of the immature HIV-1 Gag polyprotein. *Nature Struct. Biol.* **9,** 537–543 (2002).
14. Gross, I., Hohenberg, H., Huckhagel, C. & Krausslich, H. G. N-Terminal extension of human immunodeficiency virus capsid protein converts the in vitro assembly phenotype from tubular to spherical particles. *J. Virol.* **72,** 4798–4810 (1998).
15. von Schwedler, U. K. *et al.* Proteolytic refolding of the HIV-1 capsid protein amino-terminus facilitates viral core assembly. *EMBO J.* **17,** 1555–1568 (1998); corrigendum **19,** 2391 (2000).
16. Briggs, J. A. *et al.* The stoichiometry of Gag protein in HIV-1. *Nature Struct. Mol. Biol.* **11,** 672–675 (2004).
17. Lanman, J. *et al.* Identification of novel interactions in HIV-1 capsid protein assembly by high-resolution mass spectrometry. *J. Mol. Biol.* **325,** 759–772 (2003).
18. Lanman, J. *et al.* Key interactions in HIV-1 maturation identified by hydrogen-deuterium exchange. *Nature Struct. Mol. Biol.* **11,** 676–677 (2004).
19. von Schwedler, U. K., Stray, K. M., Garrus, J. E. & Sundquist, W. I. Functional surfaces of the human immunodeficiency virus type 1 capsid protein. *J. Virol.* **77,** 5439–5450 (2003).
20. Forshey, B. M., von Schwedler, U., Sundquist, W. I. & Aiken, C. Formation of a human immunodeficiency virus type 1 core of optimal stability is crucial for viral replication. *J. Virol.* **76,** 5667–5677 (2002).
21. Ganser-Pornillos, B. K., von Schwedler, U. K., Stray, K. M., Aiken, C. & Sundquist, W. I. Assembly properties of the human immunodeficiency virus type 1 CA protein. *J. Virol.* **78,** 2545–2552 (2004).
22. Fassati, A. & Goff, S. P. Characterization of intracellular reverse transcription complexes of Moloney murine leukemia virus. *J. Virol.* **73,** 8919–8925 (1999).
23. Fassati, A. & Goff, S. P. Characterization of intracellular reverse transcription complexes of human immunodeficiency virus type 1. *J. Virol.* **75,** 3626–3635 (2001).
24. Karageorgos, L., Li, P. & Burrell, C. Characterization of HIV replication complexes early after cell-to-cell infection. *AIDS Res. Hum. Retroviruses* **9,** 817–823 (1993).
25. Best, S., Le Tissier, P., Towers, G. & Stoye, J. P. Positional cloning of the mouse retrovirus restriction gene Fv1. *Nature* **382,** 826–829 (1996).
26. Boone, L. R. *et al.* Reversal of Fv-1 host range by *in vitro* restriction endonuclease fragment exchange between molecular clones of N-tropic and B-tropic murine leukemia virus genomes. *J. Virol.* **48,** 110–119 (1983).
27. Stremlau, M. *et al.* The cytoplasmic body component TRIM5α restricts HIV-1 infection in Old World monkeys. *Nature* **427,** 848–853 (2004).
28. Terwilliger, T. C. & Berendzen, J. Automated MAD and MIR structure solution. *Acta Crystallogr. D* **55,** 849–861 (1999).
29. Cowtan, K. 'dm': an automated procedure for phase improvement by density modification. *Joint CCP4 ESF-EACBM Newsl. Prot. Crystallogr.* **31,** 34–38 (1994).
30. Morris, R. J., Perrakis, A. & Lamzin, V. S. ARP/wARP and automatic interpretation of protein electron density maps. *Methods Enzymol.* **374,** 229–244 (2003).

Acknowledgements We thank S. Gamblin for assistance in crystal handling.

Competing interests statement The authors declare that they have no competing financial interests.

Correspondence and requests for materials should be addressed to I.A.T. (itaylor@nimr.mrc.ac.uk).

corrigendum

Absence of S6K1 protects against age- and diet-induced obesity while enhancing insulin sensitivity

Sung Hee Um, Francesca Frigerio, Mitsuhiro Watanabe, Frédéric Picard, Manel Joaquin, Melanie Sticker, Stefano Fumagalli, Peter R. Allegrini, Sara C. Kozma, Johan Auwerx & George Thomas

Nature **431,** 200–205 (2004).

In Fig. 4e of this Letter, the arrowhead from TSC to Rheb should be a horizontal bar (as from PKB to TSC). In addition, the phosphorylation sites of IRS1 for human should be S312 and S636/639 and for mouse the corresponding phosphorylation sites should be IRS1 S307 and S632/S635. This does not affect any of the results or conclusions of the paper. □